Research Square

Preprints are preliminary reports that have not undergone peer review.
They should not be considered conclusive, used to inform clinical practice,
or referenced by the media as validated information.

Optimization of Stepped Spillways by Studying Pressure and Turbulent Kinetic Energy

Awais Raza

awaisraza@swjtu.edu.cn

Southwest Jiaotong University

Syed Mudassir Raza

Huazhong Agricultural University

Research Article

Keywords: Cavitation, Pressure stepped spillway, Slope, Turbulent kinetic energy, Volume of fluid (VOF)

Posted Date: March 23rd, 2026

DOI: https://doi.org/10.21203/rs.3.rs-9091777/v1

License: This work is licensed under a Creative Commons Attribution 4.0 International License.
Read Full License

Additional Declarations: No competing interests reported.

Optimization of Stepped Spillways by Studying Pressure and Turbulent Kinetic Energy

Awais Raza[1], Syed Mudassir Raza[2]

[1]School of Civil Engineering, Southwest Jiaotong University Chengdu 610031, PR China (Email: *awaisraza@swjtu.edu.cn*) (corresponding author)

[2]Huazhong Agriculture University, College of Engineering, Wuhan, 430070 NX, China (E mail: *syedraza@webmail.hzau.edu.cn*)

Abstract: Pressure distribution on the step spillways is an essential factor for determining the cavitation damage in step spillways. Negative pressure at the spillway surface causes cavitation problems, so the location of negative pressure is critical in measuring the cavitation risk. Turbulent kinetic energy is also an essential consideration for measuring the intensity of turbulence over the spillway surface; for this purpose, numerical modelling is done by using four types of step spillway models by varying channel slopes (12.5°, 19°, 29°,35°) by using the volume of fluid (VOF) and realizable k-ε model. The results indicated that negative pressure occurs at the perpendicular face of the step near the edge of the step in all channel slopes. With the move up in the channel slope, the possibility of cavitation is reduced. Turbulent kinetic energy profiles rise with the surge in channel slope. Turbulent kinetic energy is increased from the crest to the bottom of the spillway. At the bottom of the spillway, turbulent kinetic energy is more like a crest. The rise in channel slope caused maximization in the turbulent kinetic energy and the air fraction profiles over the spillway surface. Air fraction profiles have a relationship with turbulent kinetic energy.

Keywords: Cavitation; Pressure stepped spillway; Slope; Turbulent kinetic energy; Volume of fluid (VOF)

1. Introduction

Mainly, stepped spillways are planned for the skimming flow regime because the skimming flow regime exists at raised discharge values. A skimming flow regime is formed when the flow rate increases and the water forms a coherent scheme. No freefall jets are formed in the skimming flow regime **Error! Reference source not found.-Error! Reference source not found.Error! Reference source not found.**. Air entrainment is significant across the skimming flow regime because the design of the stepped spillway is based on a skimming flow regime, so air entrainment is substantial for this process **Error! Reference source not found.**, **Error! Reference source not found.**. Water forms a coherent structure above the pseudo-bottom in the skimming flow regime. Pseudo-bottom is the line attaching the edges of the steps of spillways. Downstairs, the pseudo-bottom water is recirculated in circles **Error! Reference source not found.**, **Error! Reference source not found.**.

Energy loss in the skimming flow regime is primarily due to the recalculating vortices beneath the pseudo bottom. In the skimming regime, a boundary layer exists that connects the free face of the air. Air enters the water when this boundary thickness connects the free face **Error! Reference source not found.**. This start of air entrainment is essential in the skimming flow regime because cavitations, energy loss, and the span of the stilling basin depend upon this air entrainment starting **Error! Reference source not found.**. After this aerated flow region is started, the proportion of the aerated flow region is passionate about the cavitation and energy dissipation in the stepped spillways. The greater the length of the aerated flow region, the less cavitation and the more excellent the energy loss **Error! Reference source not found.**, **Error! Reference source not found.**. Primarily, scientists and engineers, while designing the stepped spillways, are established on the conditions of increasing the length of the aerated flow zone so that chances of cavitations will reduce and energy dissipation is increased due to more air entrainment **Error! Reference source not found.**, **Error! Reference source not found.**.

Energy dissipation effects with slopes are primarily measured with experiments. These investigations indicate that the steps' energy loss and air concentration depend mainly on the critical flow drop and step height (h). Critical flow depth and step height (h) are essential in energy loss in the stepped spillways. Energy dissipation over the steps is increased by changing the number of steps (N) **Error! Reference source not found.**, **Error! Reference source not found.**. Step spillways have less cavitation than smooth spillways. Leveled spillways are more vulnerable to cavitation loss. The presence of steps over the spillway surface lessens the chances of cavitation over the spillway. The occurrence of steps over the spillway face reduces the water speed over the spillway and minimizes the turbulence at the spillway's base. The span of the stilling basin was decreased by reducing turbulence at the bottom of the spillway. The span of the stilling basin is reduced in cases of step spillways **Error! Reference source not found.**, **Error! Reference source not found.**.

Numerical analysis is advantageous over prototype modelling because it gives better results with minimum expenses and no need to build a prototype model. Using computational fluid dynamics (CFD) has gained much more importance for hydraulic engineers when constructing spillways and other hydraulic structures. The complete flow data is obtained in CFD more accurately than in prototype modelling **Error! Reference source not found.**, **Error! Reference source not found.**. Qian et al. **Error! Reference source not found.** correlated the four distinct turbulent models, calculated the velocity, and compared their results with the PIV. Dong **Error! Reference source not found.** simulated the flow on the flat stepped spillway. They cast off flat spillway models and the model to analyze the spillways numerically. Morovati et al. **Error! Reference source not found.** used five types of pooled step spillways. They determined the impact of distinct pools and measured the velocity and vortex profiles over the spillway surface. Morovati and Eghbalzadeh **Error! Reference source not found.** measured the pressure and void proportion over the spillway surface utilizing Flow-3D. Wan et al. **Error! Reference source not found.** measured the inception point over the spillway surface by changing

the height and geometry of the spillway surface. Wan et al. **Error! Reference source not found.** used the wrap speed spillway model measured the cavitation loss at the spillway face. They determined that cavitation mainly occurs downstream of the spillway surface. Craft et al. **Error! Reference source not found.** used different non-linear models and different step heights for the numerical analysis of spillways. Cheng et al. **Error! Reference source not found.** used two turbulence models to render the flow over the stepped spillways. Later, they measured the RNG turbulence model to give more precise results over the other turbulence model. Using the ADINA software, Tebbara et al. **Error! Reference source not found.** analyze the flow over the stepped spillway. They used the distinct designs of steps to determine the water surface profile and measure the energy dissipation. Bai and Zhang **Error! Reference source not found.** measured the pressure codes over the three step spillways and the cavitation damage in all three sorts. Abbasi and Kamanbedast **Error! Reference source not found.** studied energy dissipation and critical depth using the Flow 3D software. Roushanger et al. **Error! Reference source not found.** used artificial intelligence and different genetic programming techniques (GEP) to calculate energy loss over the spillway surface.

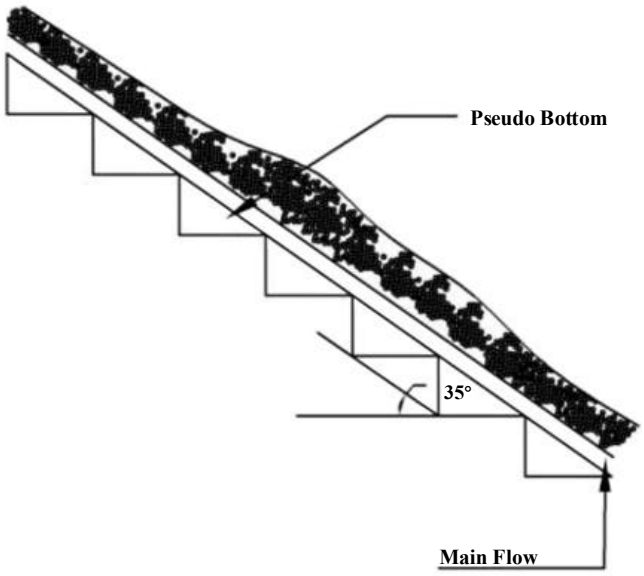


Fig. 1. Skimming flow description in different channel slope

This study is concerned with the prediction of pressure profile, turbulent kinetic energy, and air fraction profile over the step spillways by using different channel slopes varying from (19°, 29°and 35°). The scope of the study is to predict the negative pressure zone on the stepped spillway to predict the cavitation damage zone due to negative pressure. Computation fluid dynamics (CFD) using fluent multiphase (VOF) software and realizable k-ε as a turbulent model. Distinct channel slope designs are simulated at various flow rates by varying the velocity for prediction of the relationship of pressure profile, turbulent kinetic energy profile, and air volume fraction profiles with discharge and channel slope. A comparison of mean air concentration with bottom air concentration is discussed in this paper, and the effect of turbulent kinetic energy over air volume fraction is described in the paper.

2. Materials & Method

This paper uses four different channel slopes that were numerically investigated using ANSYS. The hill of spillway models varied from mild to steep slopes. The multiphase VOF and realizable k-ε model are pre-owned for turbulence modelling. A SIMPLE algorithm is adjusted to transient simulation. The momentum and turbulent kinetic energy loss rate techniques are second- and first-order upwind. PRESTO is utilized for the discretization of pressure. The data of all four models are exhibited and stated in the

Table **1**.

Table 1 Details of four models used for computation

Model	h (m)	Slope°
M_2	0.15	19°
M_3	0.24	29°
M_4	0.32	35°

2.1. Multiphase Modelling

The multiphase VOF model is used because, in this case, only two phases are involved: air and water. Hirt & Nichols (1981) give that method. When two phases are involved. The VOF is suitable when the interface location between two phases is engaged. When the VOF leads two phases, water and air, the fluid volume is regarded as 0 when it does not contain any water. The VOF is given the value of 1 when it's filled with water; if the value lies between 0 and 1, the cell is partially packed with air and partially packed with water. The properties of any cell represent one level or a mixture. All cell properties like pressure, velocity, and temperature follow the volume proportion concept. The total volume proportion in each cell is equal to unity.

The volume of fluid (VOF) method solved the different continuity and momentum equations to measure the volume proportion of each equation.

$$\frac{\partial \rho}{\partial t} + \frac{\partial \rho \mu_i}{\partial x_i} = 0 \tag{1}$$

$$\frac{\partial \rho \mu_i}{\partial t} + \frac{\partial \rho \mu_i \mu_j}{\partial x_j} = -\frac{\partial P}{\partial x_i} + \frac{\partial}{\partial x_j}(\mu + \mu_t)\left(\frac{\partial u_i}{\partial x_j} + \frac{\partial u_j}{\partial x_i}\right) \tag{2}$$

$$\frac{\partial \alpha_w}{\partial t} + \mu_i \frac{\partial \alpha_w}{\partial x_i} = 0 \tag{3}$$

Density and molecular viscosity are the attributes of volume fraction, which are not constant values; they mainly depend on the volume proportion of the water. The following equations can determine these terminologies.

$$\rho = \alpha_w \rho_w + (1-\alpha_w)\rho_a \quad (4)$$

$$\mu = \alpha_w \mu_w + (1-\alpha_w)\mu_a \quad (5)$$

In these ρ_w and ρ_a represents the density of air and water while μ_w and μ_a Represents the molecular viscosity of air and water. By repeating the solution, the ρ and μ Can be measured.

2.2 Turbulence Modelling

This paper utilizes the realizable k-ε model as a turbulence model. Realizable k-ε was introduced by Shih et al. (1994) and is used for turbulent flows because it gives better results for highly turbulent flows under the vortices. In realizable k-ε, a new equation for turbulent eddy loss is introduced derived from the high Reynolds number. The transport equation for turbulent kinetic energy (k) and turbulent eddy dissipation (ε) is below.

$$\frac{\partial}{\partial t}(\rho k) + \frac{\partial}{\partial x_i}(\rho k u_j) = \frac{\partial}{\partial x_i}\left[\left(\mu + \frac{\mu_t}{\sigma_k}\right)\frac{\partial k}{\partial x_j}\right] + G_k + G_b - \rho\varepsilon - Y_M + S_k \quad (6)$$

$$\frac{\partial}{\partial t}(\rho\varepsilon) + \frac{\partial}{\partial x_j}(\rho\varepsilon\mu_j) = \frac{\partial}{\partial x_j}\left[\left(\mu + \frac{\mu_t}{\sigma_\varepsilon}\right)\frac{\partial \varepsilon}{\partial x_j}\right] + \rho C_1 S_\varepsilon - \rho C_2 \frac{\varepsilon^2}{k + \sqrt{\upsilon\varepsilon}} + C_{1\varepsilon}\frac{\varepsilon}{k} C_{3\varepsilon} G_b + S_\varepsilon \quad (7)$$

The different equations listed below define the intended strain and rotation values, angular velocity of system spin, and turbulence fields.

$$C_\mu = \frac{1}{A_0 + A_s \dfrac{kU*}{\varepsilon}} \quad (8)$$

$$U^* = \sqrt{S_{ij}S_{ij} + \tilde{\Omega}_{ij}\tilde{\Omega}_{ij}} \quad (9)$$

$$\tilde{\Omega}_{ij} = \Omega_{ij} - 2\varepsilon_{ijk}\omega_k \quad (10)$$

$$\Omega_{ij} = \bar{\Omega}_{ij} - \varepsilon_{ijk}\omega_k \quad (11)$$

2.3. Boundary Conditions

The inlet of the spillway is the velocity inlet. The flow rate measures the velocity of the spillway. The spillway outlet is the pressure outlet, and the condition applied is that there is no backflow of the water. The spillway walls are measured as stationary walls with no slip velocity. Fig. 1 &Fig. **2** explains the systematic simulation diagram and elaborates the boundary conditions.

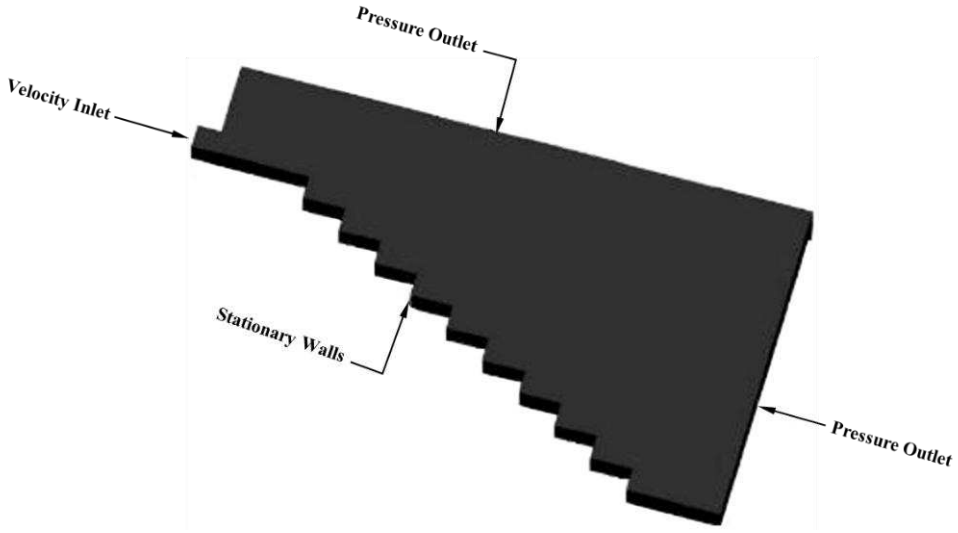
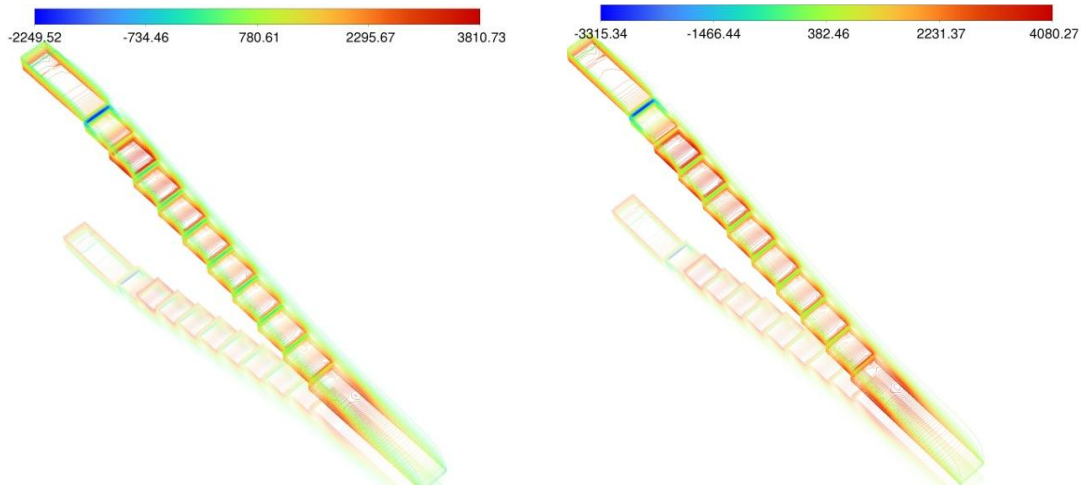


Fig. 2. Boundary Conditions and description of a model for numerical analysis

3. Results & Discussions

3.1. Pressure fluctuations' impact on various channel slopes

Fig. 3 represents the pressure contours of models at different discharges on the overall surface of a stepped spillway. Overall pressure distribution over the stepped spillway indicates that with the increase in flow value, overall pressure on the stepped spillway is increased. Also, with the rise in discharge value, overall negative pressure on the water's surface increases. It can be seen from the shape diagram that negative pressure mainly occurs over the vertical face of the step and that the pressure value is higher over the horizontal step as compared to the vertical step. Pressure values vary from step to step depending on the impact of water on the step.



(a) (b)

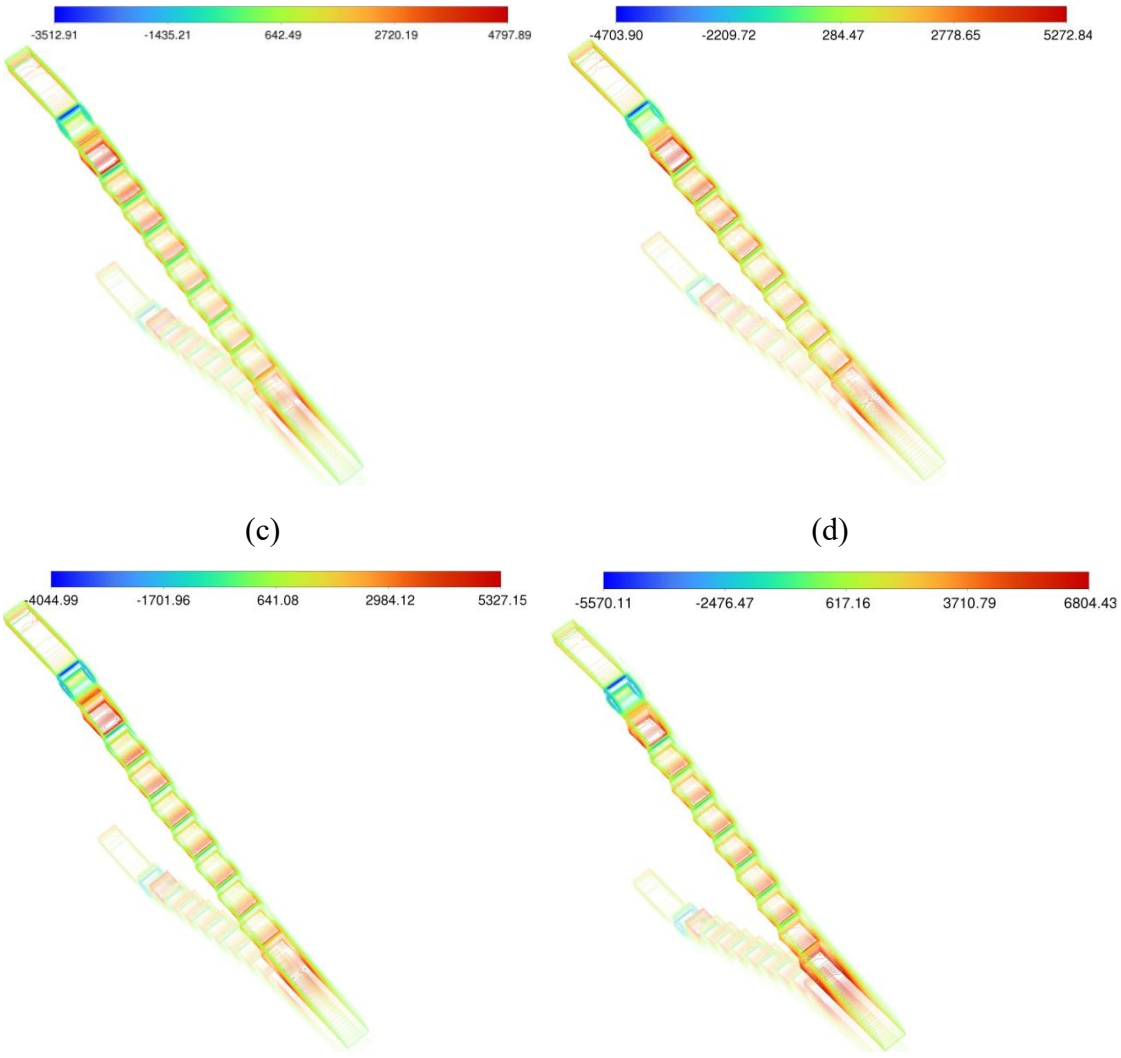
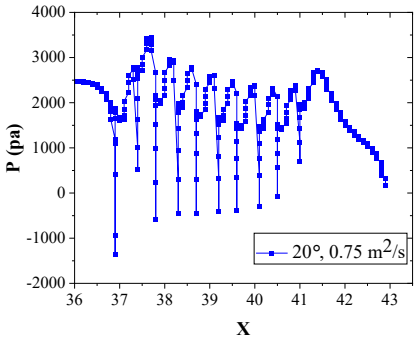
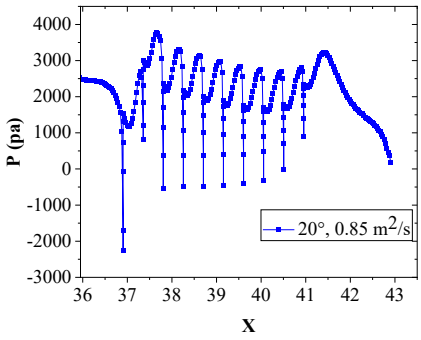


Fig. 3. Pressure contours at whole surface of stepped spillway. (a, b) pressure contours on stepped spillway with channel slope 20° at flow rate 0.875 & 1 m^2/s; (c, d) pressure contours on stepped spillway with channel slope 29° at flow rate 0.875 & 1 m^2/s; (e, f) pressure contours on stepped spillway with channel slope 35° at flow rate 0.875 & 1 m^2/s.

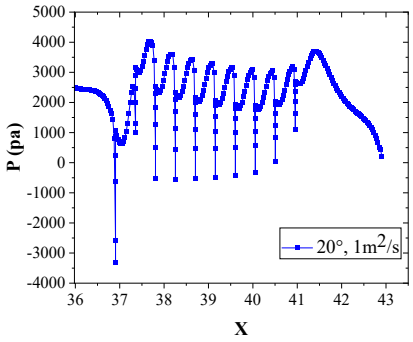
Fig. 4 represents the pressure profile at the edges of the whole spillway surface from the crest to the bottom of the spillway. Negative pressure values are displayed at the vertical edges of the step, while the loop structures give the pressure value at the horizontal step.


P (pa)
X
20°, 0.75 m2/s

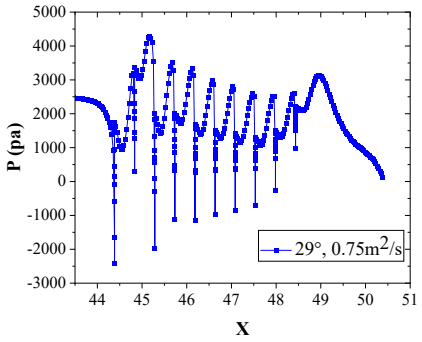
(a)


P (pa)
X
20°, 0.85 m2/s

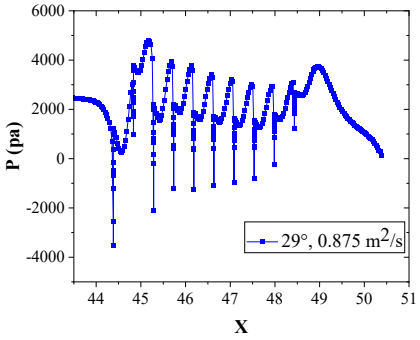
(b)


P (pa)
X
20°, 1m2/s

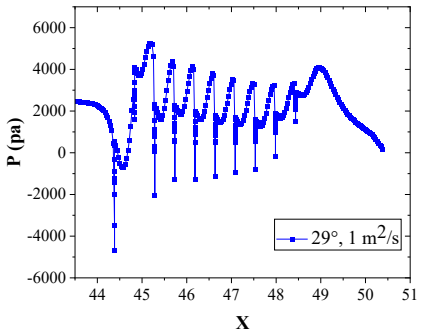
(c)


P (pa)
X
29°, 0.75m2/s

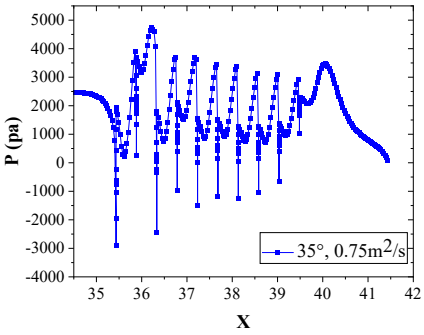
(d)


P (pa)
X
29°, 0.875 m2/s

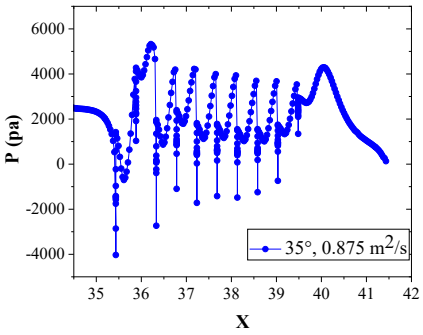
(e)


P (pa)
X
29°, 1 m2/s

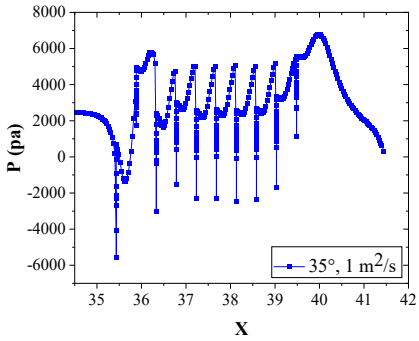
(f)


P (pa)
X
35°, 0.75m2/s

(g)


P (pa)
X
35°, 0.875 m2/s

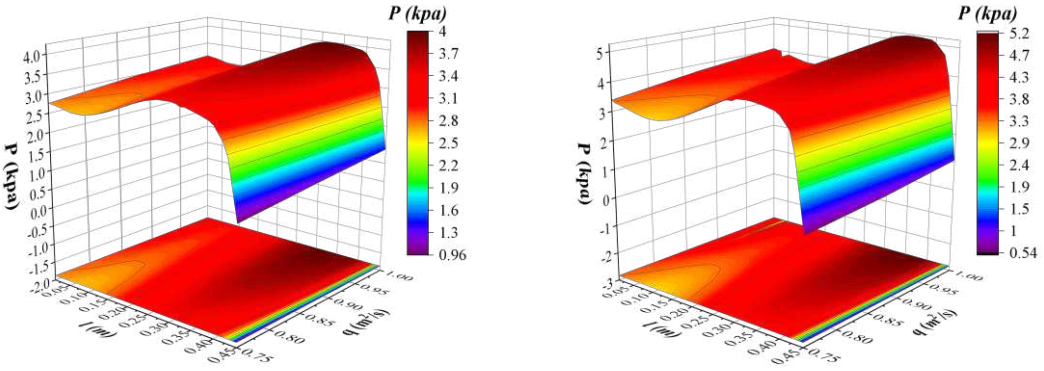
(h)



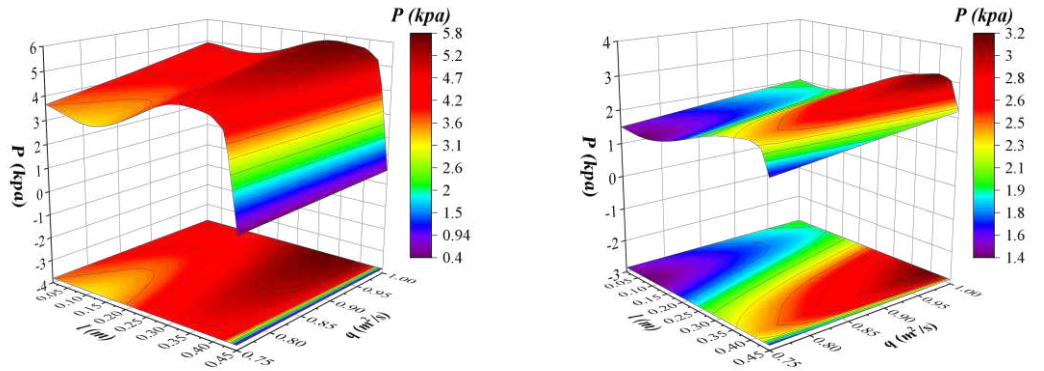
(e)

Fig. 4. Pressure profile over the spillway surface from crest to bottom of spillway at different flow rates. (a, b, c) pressure profile of 20° spillway at different flow rates of 0.75, 0.875, 1 m^2/s; (d, e, f) pressure profile of 29° spillway at different flow rates of 0.75, 0.875, 1 m^2/s; (g, h, e) pressure profile of 35° spillway at different flow rates of 0.75, 0.875, 1 m^2/s.

Fig. 5 represents the pressure propagation on the horizontal face of the 2nd and last step of all three slopes of stepped spillway models. The rise in channel slope causes the horizontal pressure to increase. The maximum pressure on the step at constant discharge is 35 degrees. The impression of pressure on the step is that it increases with distance, then declines, then rises again and reaches the maximum value, then starts declining and reaches the minimum pressure value at the border of the step. This pressure pattern is the same in all stepped spillway models at all discharge rates.



(a) (b)



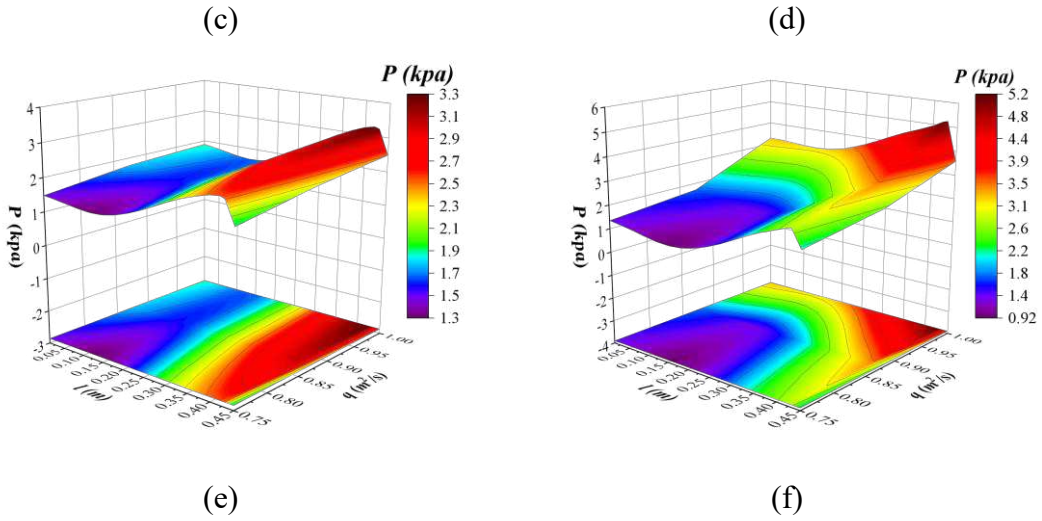
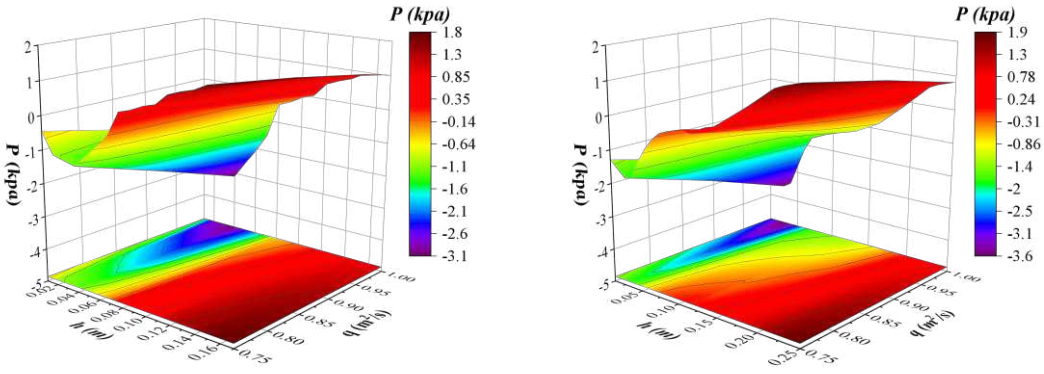
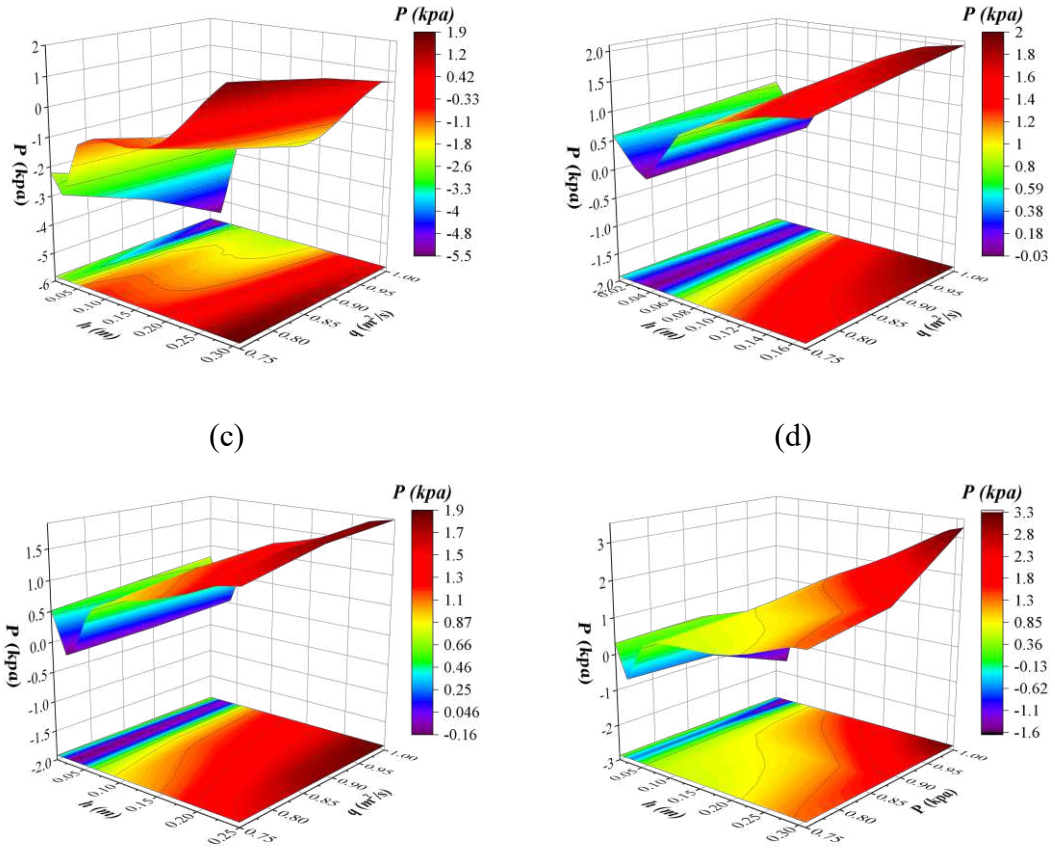


Fig. 5. 3D pressure contours on at the horizontal face of 2nd & last step with different channel slopes. (a) 3D pressure contour on the horizontal face of 2nd step with channel slope 20°; (b) 3D pressure contour on the parallel face of 2nd step with channel slope 29°; (c) 3D pressure contour on the parallel face of 2nd step with channel slope 35°; (d) 3D pressure contour on the parallel face of last step with channel slope 20°; (e) 3D pressure contour on the parallel face of last step with. channel slope 29°; (f) 3D pressure contour on the parallel face of last step with channel slope 29°.

Fig. 6 represents the vertical pressure on the second & last step. This indicates that with the increase in channel slope, pressure on the perpendicular face of the step also increases. Maximum negative pressure is occurring near the border of the step. This minimum pressure is due to the separation of recirculation from the main flow, which is raised by a rise in the discharge rate. The trend of pressure on the last vertical side of the step is reversed compared to the second step due to an aerated flow zone in the previous step. With the increase in channel slope, the curves for vertical pressure are raised, meaning that the channel slope increases the pressure codes over the perpendicular face of the step.





(c) (d)

(e) (f)

Fig. 6. 3d pressure contours at 2nd & last step of vertical face of step with different channel slopes. (a) 3d pressure contour on 2nd step at vertical face with channel slope 20°; (b) 3d pressure contour on 2nd step at vertical face with channel slope 29°; (c) 3d pressure contour on 2nd step at vertical face with channel slope 35°; (d) 3d pressure contour on last step at vertical face with channel slope 20°; (e) 3d pressure contour on last step at vertical face with channel slope 29°; (f) 3d pressure contour on last step at vertical face with channel slope 35°.

Fig. 7 represents the relative critical depth and pressure at the perpendicular face of the 2nd and last step. With the rise in critical depth, pressure at the vertical face of the step decreases, and more negative pressure appears at the border of the step for a more considerable critical depth. With the rise in relative critical depth, pressure at the vertical face of the pressure decreases.

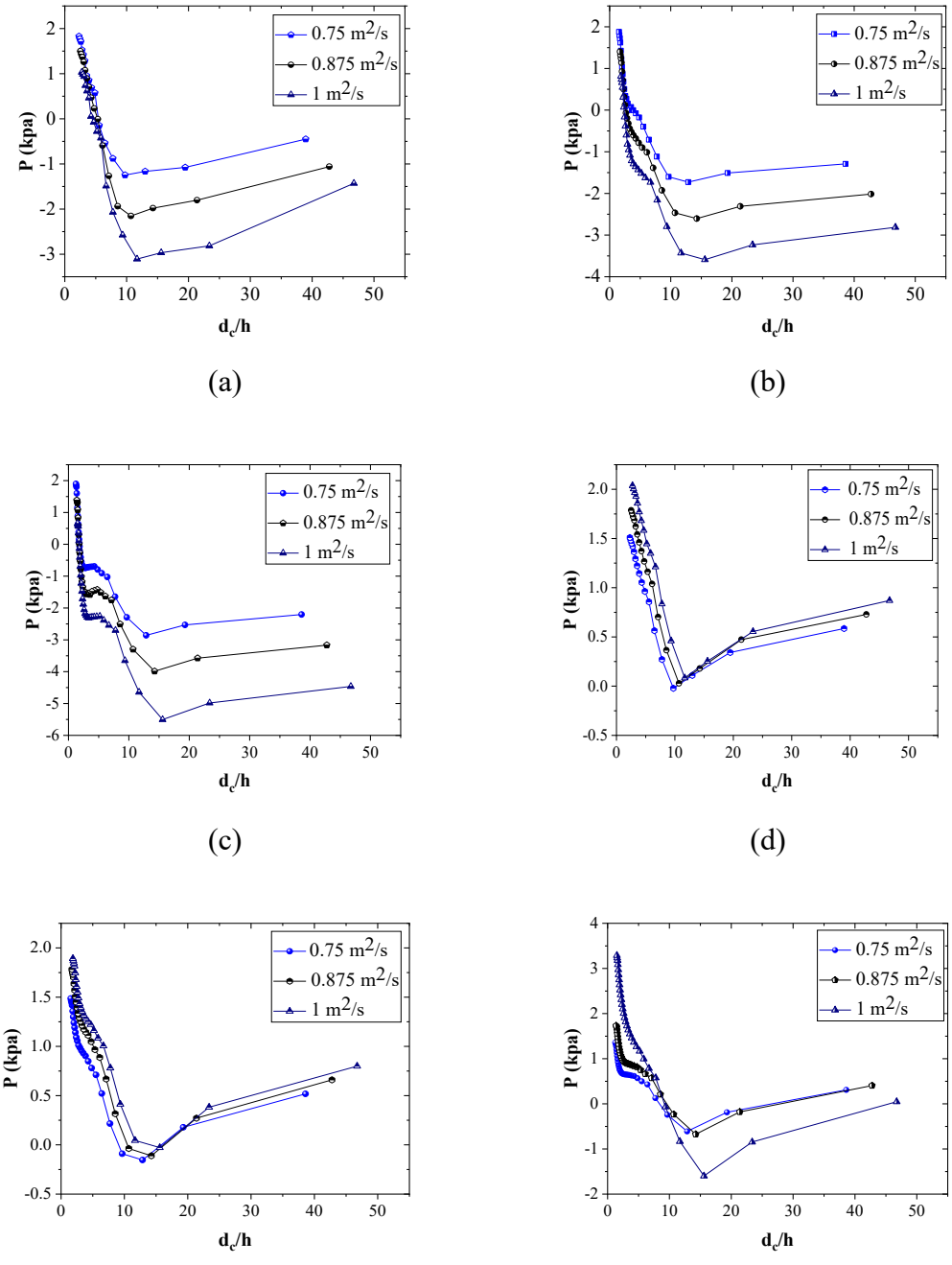


Fig. 7. Critical depth vs. pressure at 2nd vertical face of step at different channel slopes. (a) critical depth vs. pressure at 2nd vertical face of step for 20° channel slope; (b) critical depth vs. pressure at 2nd vertical face of step for 29° channel slope; (c) critical depth vs. pressure at 2nd vertical face of step for 35° channel slope; (d) critical depth vs. pressure at last vertical face of step for 20° channel slope; (e) critical depth vs. pressure at 2nd vertical face of step for 29° channel slope; (f) critical depth vs. pressure at 2nd vertical face of step for 35° channel slope.

3.2. Effects of turbulence kinetic energy with different channel slope

Fig. 8 represents the turbulent kinetic energy contours over the stepped spillways with different channel slopes for different discharges. From the contour diagram,

turbulent kinetic energy values increase during the entire step with increased discharge values. The trend of turbulent kinetic energy from top to bottom is also growing, as shown in the contour diagram. The values of turbulent kinetic energy with the increase in channel slope rise mean that the rising channel slope also increases the turbulent kinetic energy from top to bottom of the stepped spillway.

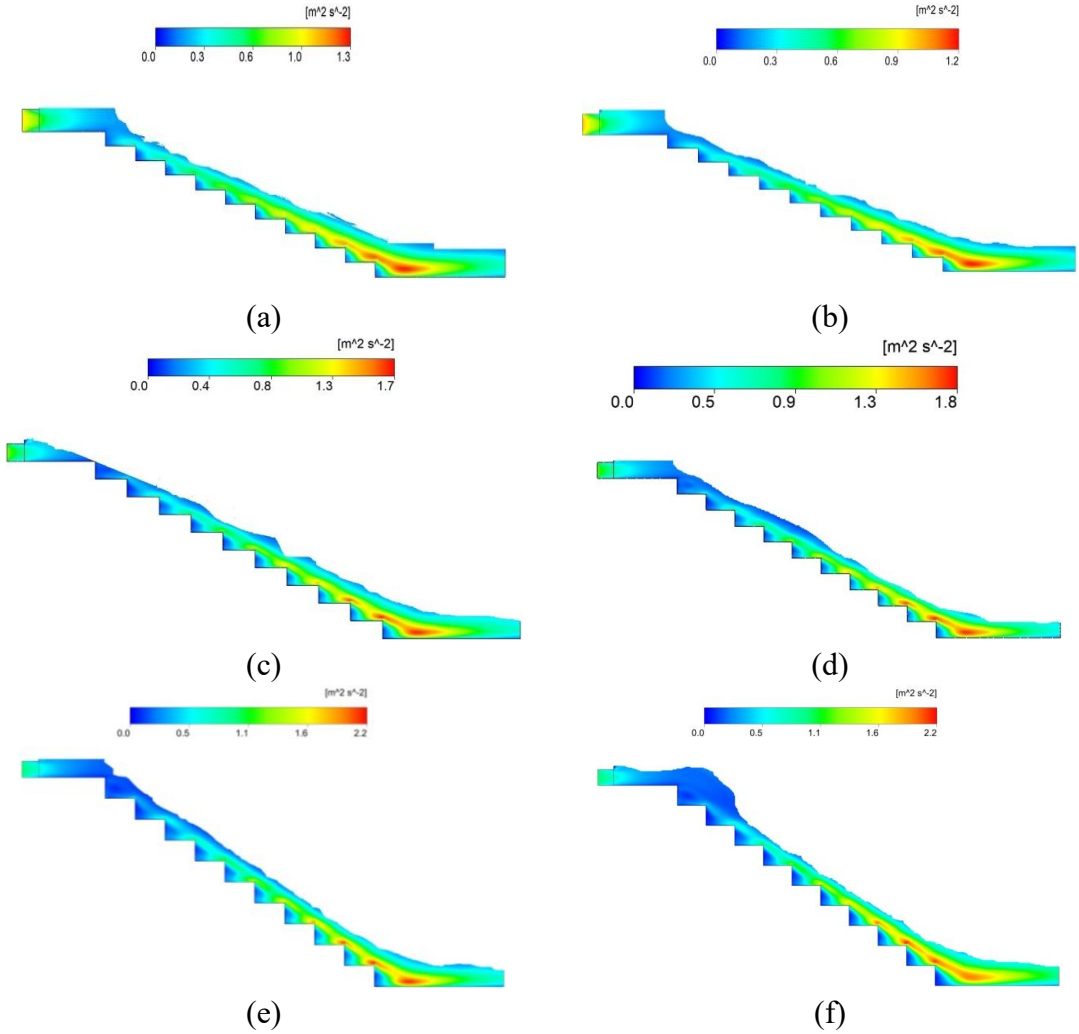


Fig. 8. Turbulent kinetic energy contours of whole spillway from top to bottom at middle of surface. (a, b) turbulent kinetic energy contours with channel slope 20° at discharge rate (0.875 & 1 m2/s); (c, d) turbulent kinetic energy contours with channel slope 29° at discharge rate (0.875 & 1 m2/s); (e, f) turbulent kinetic energy contours with channel slope 35° at discharge rate (0.875 & 1 m2/s).

Fig. 9 represents the turbulent kinetic energy profile at the horizontal and vertical face of the step from top to bottom of the spillway. With the increase in spillway slope, turbulent kinetic energy increases from the top to the bottom of the spillway. Turbulent kinetic energy shows a fluctuating trend over the spillway surface.

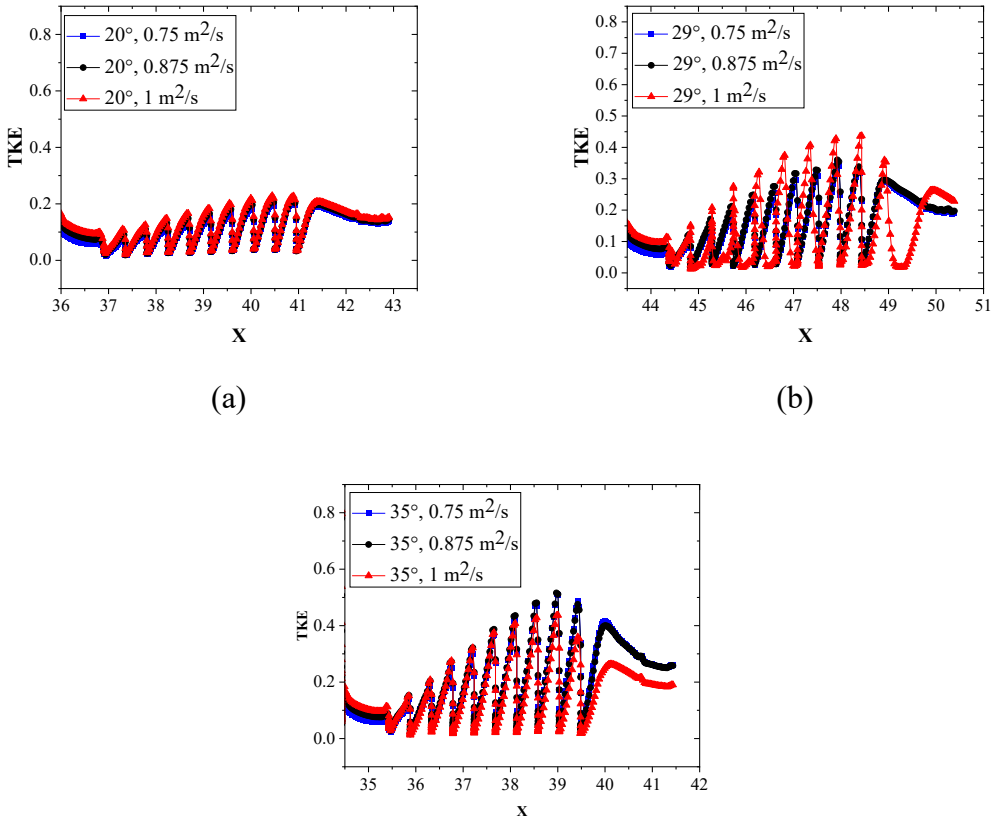
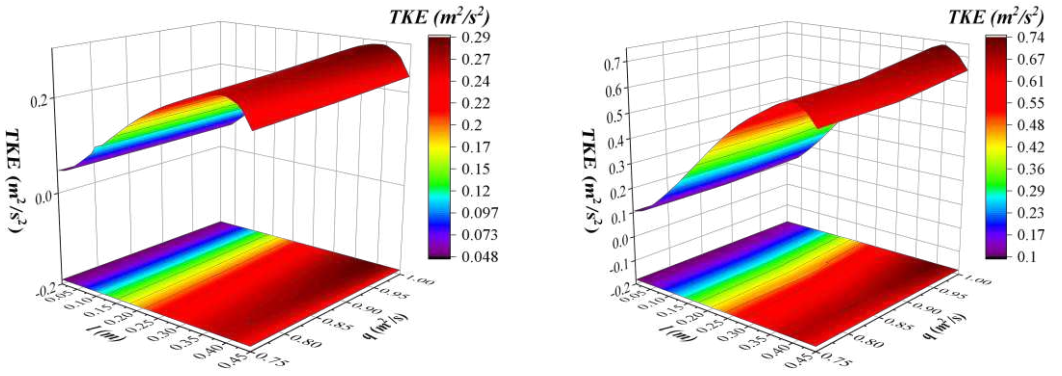
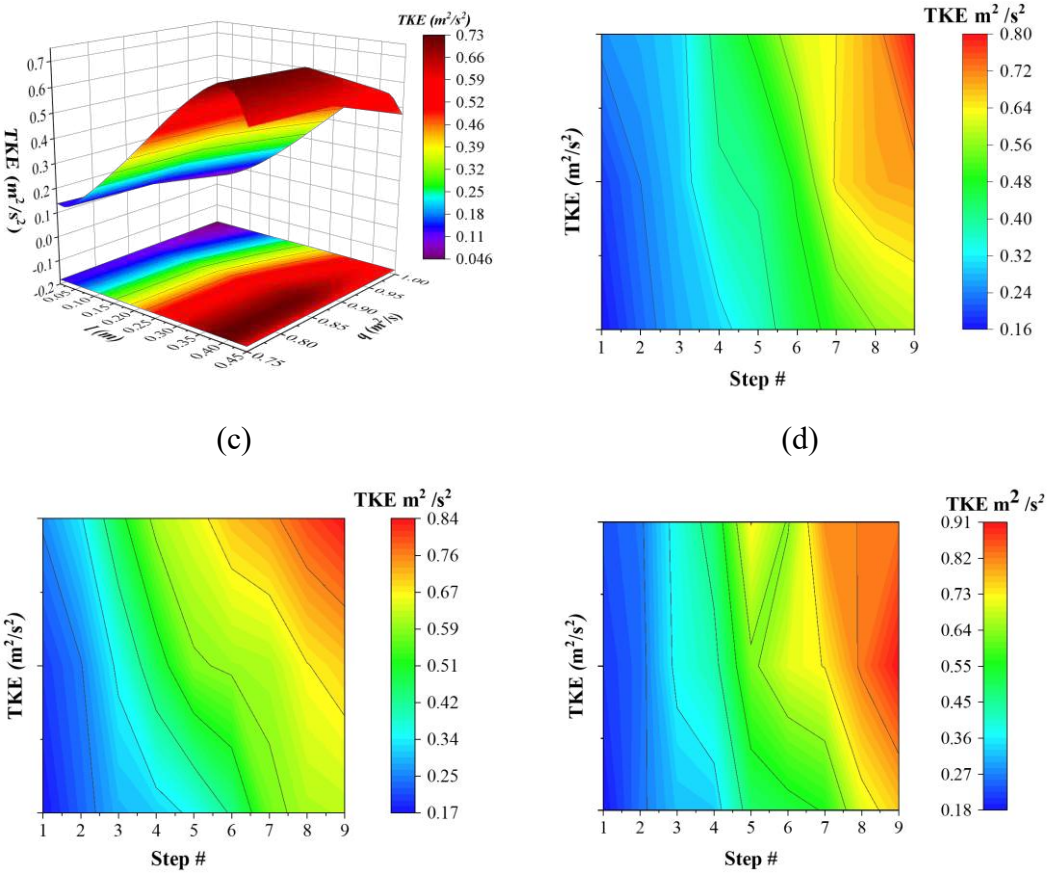


Fig. 9. Turbulent kinetic energy profile from crest to the bottom of the spillway at different flow rates. (a) turbulent kinetic energy profile of 20° spillway at different flow rates; (b) turbulent kinetic energy profile of 29° spillway at different flow rates; (c) turbulent kinetic energy profile of 35° at different flow rates.

Fig. 10 represents the turbulent kinetic energy over the last step of the horizontal face of a stepped spillway. This indicates that with the increase in horizontal distance from start to end, turbulent kinetic energy is increased, and its reach to the most significant value point near the edge of the horizontal step is reached, then again, it starts to decrease.





(c) (d)

(e) (f)

Fig. 10. 3d turbulent kinetic energy contours at the last step with different channel slopes & 2d contour graph with flow rate. (a) 3d turbulent kinetic energy contours at the previous step with channel slope 20°; (b) 3d turbulent kinetic energy contours at the last step with channel slope 29°; (c) 3d turbulent kinetic energy contours at last step with channel slope 35°; (d) 2d contours of turbulent kinetic energy with channel slope 20°; (e) 2d contours of turbulent kinetic energy with channel slope 29°; (f) 2d contours of turbulent kinetic energy with channel slope 35°.

3.3 Study of air concentration at various steps

Fig. 11 represents the air fraction profile from top to bottom at the surface of the step. At the crest of all spillways, the air fraction is almost zero. With the increase in horizontal distance, the air fraction will increase in all channel slopes. The figure mentions that the slope's rise causes an increase in air fraction. The rise of air fraction observed at the edges of each step indicates steps caused by the increase in air fraction.

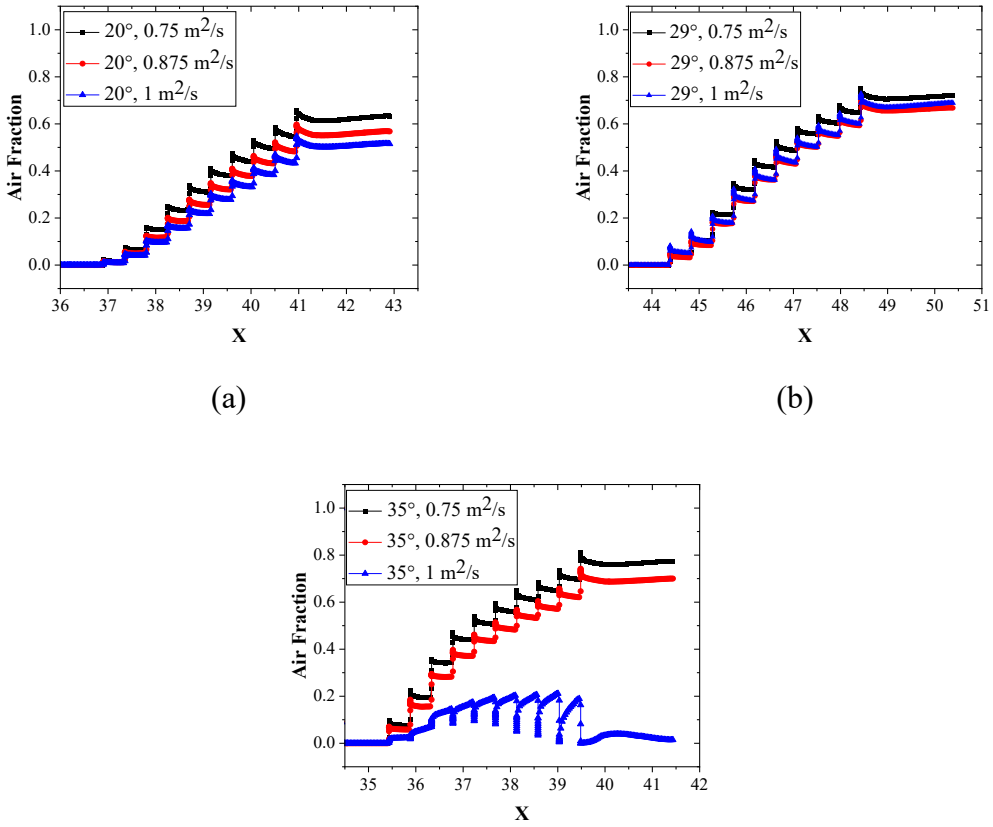


Fig. 11. Air fraction profile from crest to bottom of the spillway at different flow rates. (a) air fraction profile of 20° spillway at different flow rates; (b) air fraction profile of 29° spillway at different flow rates.

Fig. 12 represents the air concentration at the horizontal face of the 2nd and last step & of all kinds of stepped spillways with different channel slopes. The air values on the 2nd step increase with the increased channel slope. The trend of air concentration with the horizontal distance is that with the increase in horizontal distance from the start to the end of the step, air values are more significant at the beginning. It starts to decrease, then again increases at the edge of the step and reaches its maximum value. The air concentration value is higher at the start of a step than at the end. With the increase in channel slope, the quantity of air concentration at the middle of the step increases. It's clear from the contour diagram that the air concentration at the toe of a stepped spillway is higher than that at the start of the spillway. The air values at the bottom of the stepped spillway are increased due to the aerated flow zone.

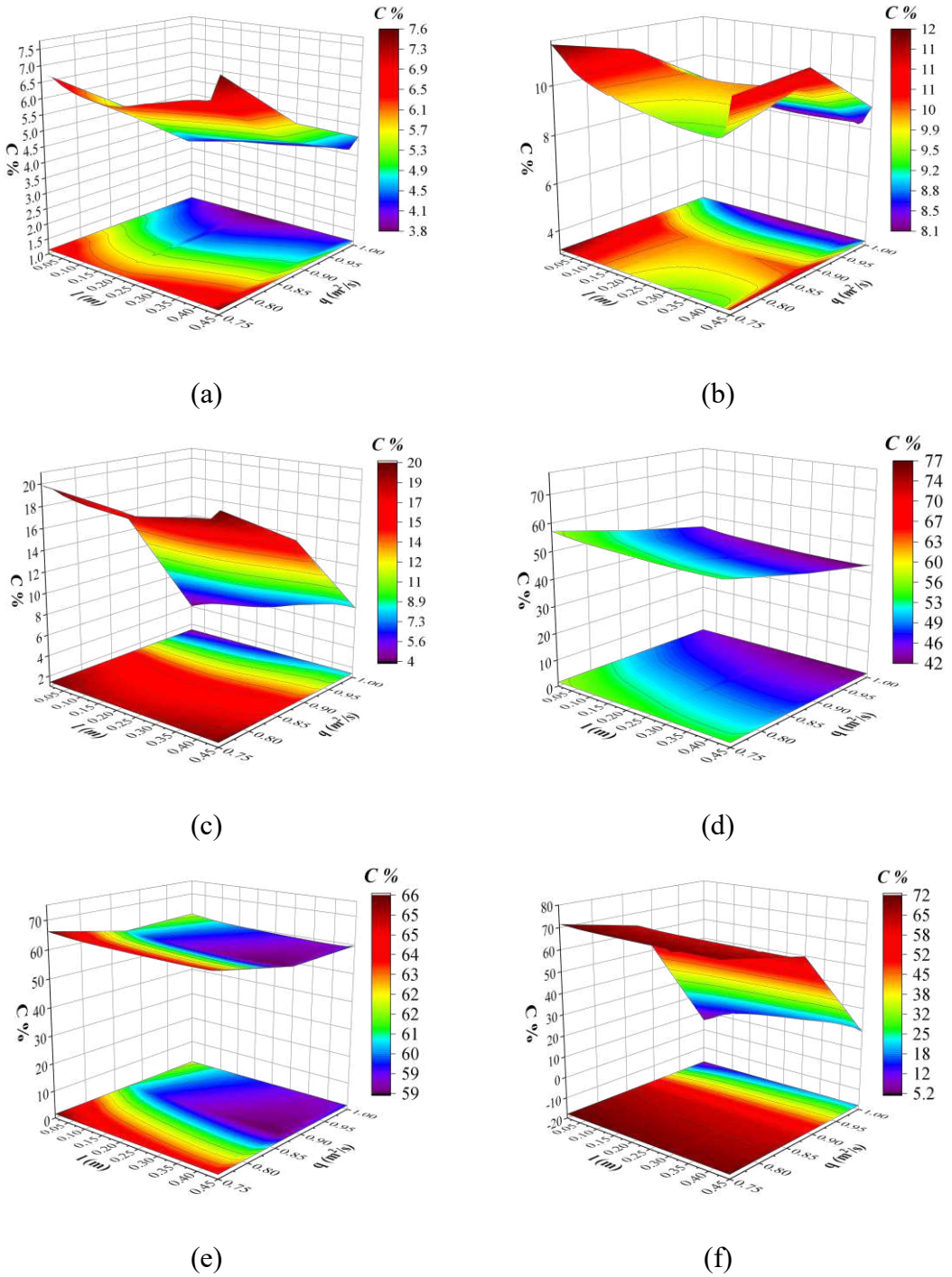
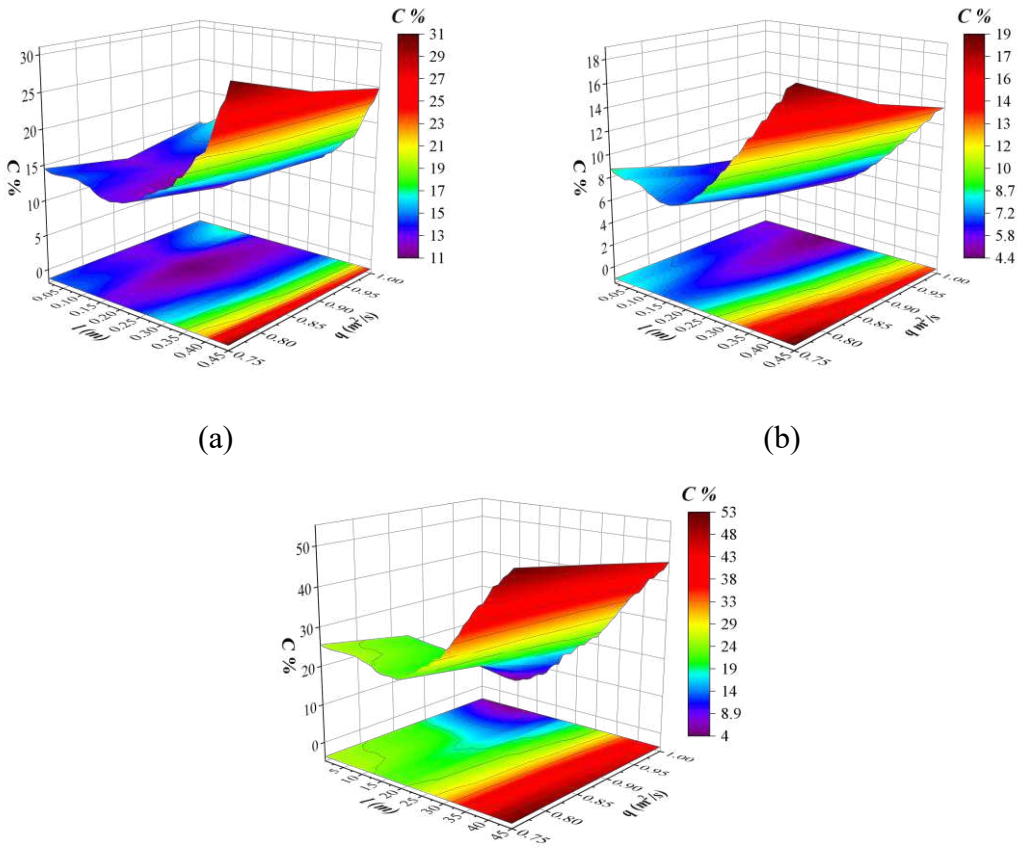


Fig. 12. 3D contours of air concentration at the bottom of 2nd step with different channel slopes. (a) 3D contours of air concentration at the bottom of step with channel slope 20°; (b) 3D contours of air concentration at the bottom of step with channel slope 29°; (c) 3d contours of air concentration at the bottom of step with channel slope 35°.

Fig. 13 represents the air concentration in the centre of the 2nd step of all stepped spillway channels at different discharges. This indicates that with the increase in distance from left to right of the step, air concentration continually decreases until it reaches its minimum value, after which it becomes constant. The continuously declining air concentration in the centre of the step surface is due to the effect of recirculation as it

decreases from left to right of the step at the middle of the step.



(a) (b)

(c)

Fig. 13. 3D contours of mean air concentration at 2nd with different channel slopes. (a) 3d contours of mean air concentration at 2nd step with channel slope 20°; (b) 3d contours of mean air concentration at 2nd step with channel slope 29°; (c) 3d contours of mean air concentration at 2nd step with channel slope 35°.

4. Conclusions

This study investigates the turbulent kinetic energy and pressure distribution over the stepped spillways by using three distinct stepped spillways with varying channel slopes and approaching numerical simulation using the VOF multiphase model and realizable k-ε to study the characteristics of turbulent kinetic energy profile, pressure distribution profile, and air volume fraction profile over the stepped spillways by varying the flow rates.

Pressure profiles over the steps in all channels are computed and discussed at different flow rates. The pressure profiles are addressed in both horizontal and vertical faces. The pressure profile of the more significant channel slope is higher than the smaller channel slope, indicating that with the increase in channel slope, the pressure profile rises over the spillway.

The negative pressure occurs adjacent to the edge of the vertical face of the step. So,

the chances of cavitation are mainly near the edges of the steps in all channel slopes. The pressure rate suddenly drops at the edge of every step and increases again at the horizontal face.

The turbulent kinetic energy profile at all three spillway models with different channel slopes is represented at various flow rates. The turbulent kinetic energy profile rises with increased channel slope and flow rate. The trend of turbulent kinetic energy increases from the crest to the toe of the spillway. At the toe of the spillway, turbulent kinetic energy is highest due to more turbulence present at the bottom.

All three models ' air fraction profiles on the spillway surface at different flow rates are discussed. The air fraction profile rises at the bottom of the spillway. From the air fraction profile, maximum air is present at the bottom of the spillway. Air fraction profiles rise with the increase in channel slope and decrease in flow rate. From profiles, it's mentioned that air concentration increases at the step's vertical edge and remains constant at the horizontal face. The mean air value at all steps is greater than the bottom air concentration. Due to more turbulence at the center of the step, the mean air concentration is higher than the bottom air concentration.

Nomenclature

A_0	constant (4.04)
A_s	constant ($\sqrt{6}\cos\phi$)
C_2	1.9 (constant)
$C_{l\varepsilon}$	1.44 (constant)
C_μ	coefficient of uniformity
G_b	generation of k due to buoyancy (kg/(ms^3))
G_k	generation of k due to fluid Shear $G_k = \mu_t S^2$ (kg/ms^3)
g	gravitational acceleration (m/sec^2)
h	step height (m)
k	turbulent kinetic energy (m^2/s^2)
l	step length (m)
M_1-M_3	stepped spillway model

335	S	modulus of the mean rate of tensor $S = \sqrt{2S_{ij}S_{ij}}$
336	S_k	source term of kinetic energy ($kg/(ms^3)$)
337	S_ε	source term of dissipation rate ($kg/(ms^4)$)
338	S_{ij}	The mean rate of deformation
339	P	pressure (N/m^2)
340	q	unit discharge (m^2/sec)
341	Y_m	Effect of compressibility on turbulence (kg/ms^3)
342	σ_k	turbulent Prandtl number
343	σ_ε	turbulent Prandtl number
344	u_i	velocity in x_i direction (m/s)
345	u_j	velocity in x_j direction (m/s)
346	α_a	volume fraction of air (%)
347	α_w	volume fraction of water (%)
348	ε	turbulent dissipation rate (m^2/sec^3)
349	θ	spillway slope (°)
350	μ	molecular dynamic viscosity (kg/ms)
351	μ_t	turbulent dynamic viscosity (kg/ms)
352	ρ	cell density (kg/m^3)
353	ρ_a	density of air (kg/m^3)
354	ρ_w	density of water (kg/m^3)
355	t	time in (sec)
356	ϕ	channel slope (°)
357	υ	kinematic viscosity (m^2/s)

dc	critical depth
$\frac{dc}{h}$	Relative critical depth
σ_k	1.0 (model constant)
σ_ε	1.2 (model constant)

Data availability

All relevant data are included in the paper.

Declaration of interests

The authors declare that they have no known competing financial interests or personal relationships that could have appeared to influence the work reported in this paper.

Funding

This research work is supported by the fundamental research funds for the central universities project grant A0920502052501.

References

Abbasi, S., & Kamanbedast, A.A. (2012). Investigation of Effect of Changes in Dimension and Hydraulic of Stepped Spillways for Maximization Energy Dissipation. *World Applied Sciences Journal*, *18*, 261 – 267. 10.5829/idosi.wasj.2012.18.02.492.

Bai, J.L., & Zhang, J.M. (2017). Comparison of Different Turbulence Models for Numerical Simulation of Pressure Distribution in V-Shaped Stepped Spillway. *Mathematical Problems in Engineering*, *2017*, 3537026. https://doi.org/10.1155/2017/3537026.

Causon, D.M., Mingham, C. G., & Ingram, D.M. (1999). Advances in calculation methods for supercritical flow in spillway channels. *Journal of Hydraulic Engineering*, *125*, 1039–1050. https://ascelibrary.org/doi/10.1061.

Christodoulou, G.C. (1993). Energy dissipation on stepped spillway. *Journal of Hydraulic Engineering*, *119*(5), 644-649. https://ascelibrary.org/doi/10.1061. Chamani, M. R., & Rajaratnam, N, (1994). Jet flow on stepped spillways. *Journal of Hydraulic Engineering*, *120*, 254 – 259. https://ascelibrary.org/doi/10.1061.

386 Chamani, M. R., & Rajaratnam, N. (1999). Characteristics of skimming flow over stepped
387 spillways. *Journal of Hydraulic Engineering*, *125*(4), 361–368.
388 https://ascelibrary.org/doi/10.1061.
389 Chinnarasri, C., & Wongwises, S. (2006). Flow patterns and energy dissipation over
390 various stepped chutes. *Journal of Irrigation & Drainage Engineering*, *132*, 70–76.
391 https://ascelibrary.org/doi/10.1061.
392 Chanson, H. (1994b). Comparison of energy dissipation between nappe and skimming
393 flow regimes on stepped chutes. *Journal of Hydraulic Research*, *32*(2), 213–218.
394 https://doi.org/10.1080/00221686.1994.10750036.
395 Chanson, H. （1994）. Hydraulics of skimming flows over stepped channels and
396 spillways. *Journal of Hydraulic Research*, *32*, 445–460.
397 https://doi.org/10.1080/00221689409498745.
398 Chanson, H. (1996). Prediction of the transition nappe/skimming flow on a stepped
399 channel. *Journal of Hydraulic Research*, *34*, 421–442.
400 https://doi.org/10.1080/00221689609498490.
401 Chanson, H. (1997). *Air Bubble Entrainment in Free-Surface Turbulent Shear Flows*.
402 London, UK: Academic Press, 401.
403 https://www.sciencedirect.com/book/9780121681104.
404 Chanson, H. (1995a). History of stepped channels and spillways. *Canadian Journal of*
405 *Civil Engineering*, *22*(2), 247–259. https://doi.org/10.1139/l95-034.
406 Chanson, H, （2001a）. Historical development of stepped cascades for the dissipation
407 of hydraulic energy. *Transactions of Newcomen Society*, *71*(2), 295–318.
408 https://doi.org/10.1080/03720187.2000.12023617.
409 Chanson, H,（2001b）. The hydraulics of stepped chutes and spillways. In: A.A. Balkema,
410 Lisse, the Netherlands. https://doi.org/10.1115/1.1523365.
411 Pravdivets, Y. P, 1993. Stepped spillways in the world and domestic hydraulic
412 engineering. *Hydrotechnical Construction*, *27*(10), 589–594.
413 https://link.springer.com/article/10.1007/BF01545067.
414 Chatila, J.G., & Jurdi, B.R. (2004). Stepped spillway as an energy dissipater. *Canadian*
415 *Water Resources Journal*, *29*(3), 147–58. https://doi.org/10.4296/cwrj147. Cheng, X.,
416 Chen, Y., & Luo, L. (2006). Numerical simulation of air-water two-phase flow over
417 stepped spillways. *Science China Technological Sciences*, *49*, 674–684.
418 https://www.mdpi.com/2073-4441/11/10/1956.
419 Craft, T. J., Launder, B. E., & Suga, K. (1996). Development and application of a cubic
420 eddy-viscosity turbulence model. *International Journal of Heat and Fluid Flow*, *17*,
421 108–111. https://doi.org/10.1016/0142-727X(95)00079-6.
422 Felder, S, （2013）. *Air-Water Flow Properties on Stepped Spillways for Embankment*
423 *Dams: Aeration, Energy Dissipation and Turbulence on Uniform, Non-Uniform and*
424 *Pooled Stepped Chutes*. School of Civil Engineering, University of Queensland,
425 Brisbane, Australia. https://espace.library.uq.edu.au/view/UQ:301329.

Dong, Z.Y. (2006). Numerical simulation of skimming flow over the mild stepped channel. *Journal of Hydrodynamics, 18*, 367 – 371. https://doi.org/10.1016/S1001-6058(06)60018-8.

Matos, J., & Frizell, K.H. (2000). *Air Concentration and Velocity Measurements on Self-Aerated Flow Down Stepped Chutes.* In: Proceedings of the 2000 Joint Conference on Water Resource Engineering and Water Resources Planning & Management, Minneapolis, MN, USA. https://ascelibrary.org/doi/10.1061/4051.

Meireles, I., & Matos, J, (2009). Skimming flow in the non-aerated region of stepped spillways over embankment dams. *Journal of Hydraulic Engineering*, *135*, 685 – 689. https://ascelibrary.org/doi/10.1061/4051.

Morovati, K., Eghbalzadeh, A., & Soori, S. (2016). Numerical Study of Energy Dissipation of Pooled Stepped Spillways. *Civil Engineering Journal, 2*, 208 – 220. https://doi.org/10.28991/cej-2016-00000027.

Morovati, K., & Eghbalzadeh, A. (2018). Study of inception point, void fraction and pressure over pooled stepped spillways using Flow-3D. *International Journal of Numerical Methods for Heat & Fluid Flow, 8*, 982-998. https://www.emerald.com/insight/content/doi/10.1108/hff-03-2017-0112.

Qian, Z.D., Hu, X.Q., Huai, W.X., & Amador, A. (2009). Numerical simulation and analysis of water flow over stepped spillways. *Science in China Series E: Technological Sciences, 52*, 1958 – 1965. https://link.springer.com/article/10.1007/s11431-009-0127-z.

Roushangar, K., Akhgar, S., Salmasi, F., & Shiri, J, (2017). Neural networks- and neuro-fuzzy-based determination of influential parameters on energy dissipation over stepped spillways under nappe flow regime. *Journal of Hydraulic Engineering*, *23*, 57-62. https://doi.org/10.1080/09715010.2016.1235472.

Salmasi, F., Poorescandar, S., Dalir, A., & Farsadi, Z.A. (2012). Discharge relations for rectangular broad-crested weirs. *Journal of Agricultural Sciences*, *17*(4), 324-336. https://doi.org/10.1501/Tarimbil_0000001184.

Tufim, A. (2010). Solution for spillway flow by finite difference method. *Journal of Hydraulic Research*, *39*, 241 – 247. https://doi.org/10.1080/00221680109499827.

Tabbara, M., Chatila, J., & Awwad, R. (2005). Computational simulation of flow over stepped spillways. *Journal of Computers Structures*, *83*, 2215 – 2224. https://doi.org/10.1016/j.compstruc.2005.04.005.

Wan, W., Raza, A., & Chen, X. (2019). Effect of Height and Geometry of Stepped Spillway on Inception Point Location. *Applied Sciences*, *9*, 2091. https://www.mdpi.com/2076-3417/9/10/2091.

Wan, W., Liu, B. & Raza, A. (2018). Numerical Prediction and Risk Analysis of Hydraulic Cavitation Damage in a High-Speed-Flow. *Shock & Vibrations*, 1817307. https://onlinelibrary.wiley.com/doi/10.1155/2018/1817307.